Soft Matter

Accepted Manuscript

ROYAL SOCIETY OF CHEMISTRY

www.rsc.org/softmatter

Impact of Cellulose Nanocrystals on the Aggregation and Initial Adhesion of *Pseudomonas fluorescens* Bacteria

Xiaohui Sun[1], Qingye Lu[1], Yaman Boluk[1,2], Yang Liu[1,*]

[1]Department of Civil and Environmental Engineering, Faculty of Engineering, University of Alberta, Edmonton, AB, T6G 2W2, Canada

[2]National Institute for Nanotechnology, National Research Council of Canada, Edmonton AB T6G 2M9, Canada

* To whom correspondence should be addressed: Email: yang.liu@ualberta.ca, Phone: 780-492-5115 Fax: 780-492-0249

Abstract

Deposition on silica surfaces of two *Pseudomonas fluorescens* strains (CHA0 and CHA19-WS) having different extracellular polymeric substance (EPS) producing capacities, was studied in the absence and presence of cellulose nanocrystals (CNC). Batch (batch soaking) and continuous flow (quartz crystal microbalance with dissipation) methods were used to evaluate the impact of CNC on bacterial initial adhesion. This study demonstrated that bacterial initial adhesion to solid surfaces can be significantly hindered by CNC using both methods. In the presence of CNC, it was observed that bacteria with more EPS aggregated more significantly compared to bacteria with less EPS, and that bacterial deposition in this condition decreased to a greater extent. The classic DLVO theory failed to predict bacterial adhesion behavior in this study. A detailed discussion is provided regarding potential antibacterial adhesion mechanisms of CNC.

Keywords: cellulose nanocrystals (CNC), bacterial aggregation**,** bacterial initial adhesion, extracellular polymeric substance (EPS).

Introduction

Bacterial adhesion and biofilm development on solid surfaces is a survival strategy employed by virtually all bacteria. However, biofilm formation in aqueous environments can be detrimental to both human life and industrial processes and should be well controlled [1]. For instance, biofilms and bioflocs need to be removed from medical devices to prevent bacterial infection and from drinking water distribution pipes and unit operations to avoid biofouling. It is important to be able to control bacterial attachment and biofilm formation in natural and engineered systems.

The initial attachment of bacteria to a surface is a key preliminary step in biofilm formation because this process has a major impact on subsequent bacterial growth, extracellular polymeric substances (EPS) production, later bacterial adhesion, and biofilm formation. Aggregation and adhesion of bacteria, like that of inert colloids, depend on van der Waals forces, electrostatic interactions, hydrophobic interactions, hydration, steric forces, and other specific forces existant between bacterial cells and surfaces [2]. The complex and heterogeneous surface structures of bacteria, such as their surface appendages, can complicate the interaction between bacteria and substratum surfaces [3]. Bacterial surface appendages, such as EPS, are believed to influence bacterial aggregation and adhesion [4]. Bacterial adhesion to a solid surface consists of two major steps. First, bacterial cell transport to a solid surface is controlled by the size of the cells and the hydrodynamics of the system. Second, when a cell and a surface are in close proximity, the subsequent interaction can be determined by DLVO (Derjaguin-Landau-Verwey-Overbeek)-type interactions, hydrophobic, and hydration interactions [5].

Moreover, in the flow regime (simple shear systems), fluid drag effects (shear forces) on bacterial deposition should be taken into account.

Our previous study showed that rod-shaped cellulose nanocrystals **(**CNC), even at low concentration (relative to the model prediction), are effective in agglomerating gram-negative EPS producing bacteria *Pseudomonas aeruginosa* PAO1 through a depletion mechanism [6]. The depletion force between particles was first recognized and described theoretically by Asakura and Oosawa [7]. When small particles such as CNC are added to a colloidal dispersion of large particles such as a bacterial culture, a depletion interaction can lead to the exclusion of small particles from the gaps between the large particles. This exclusion occurs due to a difference between the osmotic pressures in the gaps and in the bulk solution. It has been suggested that the presence of EPS on *P. aeruginosa* PAO1 cell surfaces contributes to the low CNC concentrations needed to cause bacterial depletion aggregation [6]. Other physicochemical factors, such as solution chemistry and the presence of multivalent ion species may also play an important role in bacterial aggregation and adhesion [5, 8].

However, it is unclear how CNC-induced bacterial aggregation might depend on the capacity of bacerial cells to produce EPS, and how CNC influence bacterial adhesion in aqueous environments. Hereby, the overall objective of this study was to evaluate the impact of CNC particles on the aggregation and initial ahesion of bacterial cells with different EPS-producing capabilities.

CNC are a newly developed, biodegradable, environmentally friendly rod-shaped nanoparticles. CNC increase the strength and stiffness of materials to which they are added, and are therefore used in coatings, films, textiles, and reinforcing fillers. However,

the impact of CNC on bacterial initial adhesion to surfaces has never been evaluated. In this study, the aggregation of bacteria in the absence and presence of CNC was assessed by microscopy and the deposition of bacteria on solid surfaces in the absence and presence of CNC was determined using a batch method and a continuous flow method using a quartz crystal microbalance with dissipation (QCM-D). Microscopy was used to quantify cell deposition.

Materials and methods

Culture and characterization of bacteria

Green fluorescent protein (GFP) labeled gram-negative strains of *Pseudomonas fluorescens*, wild type (*P. flu* CHA0, with normal EPS production) and the mutant Δ*gacS* that can overproduce cellulose in their EPS (*P. flu* CHA19-WS, with increased EPS production; WS [wrinkly spreader] indicates one colony morphology variant from biofilms of the Δ*gacS* strain) were selected to perform bacterial aggregation and adhesion experiments. For each experiment, the two strains of *P. flu* CHA0 and *P. flu* CHA19-WS were each streaked onto an Luria-Bertani (LB) agar plate and then incubated at 30 °C overnight. A single colony from each plate was transferred into 50 mL of LB broth and grown in a shaker incubator at 150 rpm at 30 °C overnight. Stationary-phase bacterial cells were harvested by centrifugation at 3000 g at 4 °C for 10 minutes. The growth medium was decanted, and the pellets were resuspended in 10 mM NaCl prepared with reagent grade salt (Fisher Scientific Inc., U.S.) and Milli-Q water (18.2 MΩ, Millipore, Mississauga, ON, Canada) with no pH adjustment (pH 6.0–6.2) and sterilized by autoclave before use. All characterizations and experiments were conducted using these

cell suspensions. Centrifugation and resuspension procedures were repeated two additional times to remove traces of growth media and suspended EPS from the solutions. A final cell density of 1.0×10^8 cells·mL^{-1} was obtained by measuring the optical density (OD) at 600 nm with a UV spectrophotometer (Varian Inc., U.S.). Scanning electron microscopy (SEM) was employed to characterize the size and morphology of the bacterial cells. The zeta potential and average hydrodynamic size of each strain were determined by dynamic light scattering (DLS) (Malvern Zetasizer Nano-ZS. Model: ZEN3600, Malvern Instruments Ltd, Worcestershire, UK) at 25 °C. Zeta potential and particle size measurements were repeated in five independent experiments.

CNC suspension: preparation and characterization

A stock suspension of 1.0% (wt) CNC was prepared right before each experiment by suspending CNC particles in 10 mM NaCl, pH 6.0–6.2, and sonicating the solution for 5 minutes in a ultrasonic bath to disperse the CNC particles. The CNC suspension was then filtered through a 0.45 μm membrane (Acrodisc® Syringe Filters with GHP Membrane, Pall Corporation, US) and used directly in bacterial aggregation and adhesion experiments. The size and zeta potential of the CNC particles were assessed by DLS measurements in 10 mM NaCl at 25 °C. The size was then qualitatively compared with images from transmission electron microscopy (TEM).

Bacterial aggregation experiments

In the aggregation experiment, 1 mL 1.0% (wt) CNC suspension was added to 1 mL of the bacterial suspension to achieve a volume fraction of 3.3×10^{-3} mL·mL^{-1} (detailed

calculations of volume fraction are provided in the Supporting Information). Treatment controls without added CNC were also prepared. The whole system was incubated statically at 24 °C for 30 minutes before bacterial cells were dropped on clean microscopy glass slides (Fisher Scientific) (the cleaning protocal is provided in the Supporting Information) to facilitate fluorescent microscopic observations. Microscopic visualization of the slides was carried out under fluorescent light using an Axio Imager M2 microscope (Carl Zeiss, Germany) with a Zeiss LD Plan-NEOFLUAR 40× objective. At least 10 randomly chosen areas of each slide were imaged; the number and size (radius) of bacterial aggregates in each area were obtained through counting the aggregates in 10 areas and averaging the results. These experiments were conducted in triplicate in at least five independent experiments.

Bacterial initial adhesion experiments: Batch method

To evaluate and quantify the impact of CNC on bacterial initial adhesion, a batch method [3] was employed by immersing a clean microscopy glass cover slip (Fisher Scientific) in each bacterial suspension. For each adhesion experiment, fresh *P. flu* CHA0 and *P. flu* CHA19-WS bacterial suspensions (1.0×10^8 cells·mL^{-1} in 10 mM NaCl) were prepared. 1 mL was distributed in each well of a 24-well plate (Corning Inc., U.S.) and then 1 mL of 1.0 % (wt) CNC suspension (in 10 mM NaCl) was added to each well to achieve a volume fraction of 3.3×10^{-3} mL·mL^{-1} The cleaned glass cover slips were completely submerged in the bacterial suspensions, the whole system was placed in a shaker incubator for 30 minutes at 24 °C and 120 rpm. The glass cover slips were removed from the bacterial suspensions and rinsed with 10 mM NaCl solution to remove loosely

attached cells. To observe the difference before and after CNC treatment of each strain, the cells attached to the slides were visualized and quantified by fluorescence microscopy. Briefly, after each adhesion test, the bacteria coated slides were placed on clean microscope slides. At least 50 randomly chosen areas on each slide were imaged with fluorescent light with a 40× objective. The size of each image was 3.7632×10^{-4} cm^2. The cell density (cells·cm^{-2}) on each slide was obtained through counting the cells in each area, then taking the average of all of the area cell counts. Batch bacterial adhesion experiments were conducted in duplicate in at least five independent experiments. The variance of bacterial adhesion was analyzed with a one-way analysis of variance (ANOVA) and was reported as p-values. p-values of less than 0.05 suggested that differences were statistically significant.

Bacterial initial adhesion experiments: Continuous flow method

To mimic environmentally relevant flow conditions, and to evaluate real-time bacteria-surface interactions, a continuous flow method was applied using a quartz crystal microbalance with dissipition (QCM-D). QCM-D is an advanced technology for the study of surface interactions and provides real-time, label-free measurements of molecular adsorption and/or interactions taking place on surfaces. Based on the piezoelectric effect, the frequency change (ΔF) of a quartz crystal sensor corresponds to the mass loaded on the quartz surface; the dissipation change (ΔD) indicates the energy dissipation response of the freely oscillating sensor and corresponds to the viscoelastic properties of molecular layers as they build up or are otherwise changed on the quartz surface. The QCM-D technique is sensitive to nanograms of mass and can be applied to

in situ structural arrangements, thus it is a useful technique to investigate the mechanisms and strength of cell adhesion to surfaces [9-12].

Deposition of bacteria on silica coated quartz surfaces (with a fundamental resonant frequency of approximately 5 MHz, QSX-303, Q-sense AB, Gothenburg, Sweden) was studied using a QCM-D (Q-sense E4, Biolin Scientific, Sweden). All QCM-D experiments were performed under flow-through conditions, using a digital peristaltic pump (ISMATEC, IPC high precision multichannel dispenser) operating in pushing mode, with the studied solutions injected into the sensor crystal chamber at 0.15 mL·min^{-1} [13, 14]; the temperature within each flow module was maintained at 24 °C. According to the manufacturer, such a flow rate results in laminar flow through each flow module. Prior to each experiment, the cleaned silica surface was equilibrated by pumping 10 mM NaCl solution through it. The 1.0% CNC suspension, the bacterial suspension, and the bacterial suspension supplemented with CNC (5 mL bacteria suspension in 10 mM NaCl plus 5 mL 1.0 % CNC in 10 mM NaCl) were then each injected for 30 minutes to assess the bacterial deposition behavior. Following the injection, silica surfaces were eluted with 10 mM NaCl to assess bacterial adhesion stability.

To further investigate the impact of CNC on bacterial deposition, QCM-D experiments were also conducted using CNC coated silica surfaces. Prior to each experiment, the cleaned silica surface was equilibrated by pumping 10 mM NaCl solution through it. The 1.0% CNC suspension was then injected for 20 minutes to coat the silica surface. Following the injection, silica surfaces were eluted with 10 mM NaCl to assess CNC deposition stability. Bacterial suspension was then injected for 20 minutes to assess the

bacterial deposition behavior. QCM-D experiments were repeated in at least five independent experiments, and representative results were presented in results section.

Microscopy images of the silica surfaces were captured after the QCM-D adhesion experiments to quantify adhered cell numbers. The cell density (cells·cm^{-2}) on the silica surfaces was calculated based on the microscopy images. In contrast to the batch systems, QCM-D experiments allow continuous, noninvasive monitoring of bacterial adhesion, which reflects the natural environment where the organisms reside.

DLVO interaction energy calculations

The initial adhesion of bacteria to solid substrata in aquatic systems is considered to be similar to the deposition of colloidal particles. Thus, classic DLVO theory has been widely applied to explain bacterial adhesion behavior [15-17]. Classic DLVO theory describes the total energy ΔG^{TOT} between bacteria and substratum in solution as a balance between attractive Lifshitz-van der Waals ΔG^{LW} and electrostatic ΔG^{EL} interaction free energies as a function of separation distance d [18-20], as expressed in Equation 1.

$$\Delta G^{TOT}(d)_{classical} = \Delta G^{LW}(d) + \Delta G^{EL}(d) \quad (1)$$

Sphere-plate geometry was assumed when calculating the interaction energies between the bacteria and surface (the cells are assumed to be spherical, with radius of a, approaching a semi-infinite plate). The free energies—$\Delta G^{LW}(d)$ and $\Delta G^{EL}(d)$— involved in this process are expressed in Equation 2:

$$\Delta G^{LW}(d) = -\frac{A_{123}a}{6d}$$

$$\Delta G^{EL}(d) = \pi\varepsilon a(\zeta_1^2 + \zeta_2^2)\left[\frac{2\zeta_1\zeta_2}{\zeta_1^2 + \zeta_2^2}\ln\frac{1+\exp(-\kappa d)}{1-\exp(-\kappa d)} + \ln\{1-\exp(-2\kappa d)\}\right] \quad (2)$$

A_{123}, ε, ζ, and κ^{-1} are the un-retarder bacterium-water-substratum Hamaker constant in water, the permittivity of the medium, the zeta potential, and the Debye length, respectively. *d* is the separation distance between the bacterium and the substratum. The input parameters needed to describe the electrostatic and van der Waals forces for bacterium-silica and CNC-silica interactions are provided in Table S1 in the Supporting Information.

Results

Characterization of bacterial cells and CNC particles

The wild type strain *P. flu* CHA0 is reported to have normal EPS production, whereas the mutant strain *P. flu* CHA19-WS has increased EPS production. As shown in Figure 1, both strains are rod-shaped and equipped with thread-like EPS appendages. More EPS coverage was observed on *P. flu* CHA19-WS (Figure 1B) than on *P. flu* CHA0 (Figure 1A). The results are consistent with the fact that *P. flu* CHA19-WS cells overproduce cellulose in their EPS [21]. DLS measurements showed that the hydrodynamic diameter of *P. flu* CHA0 cells, 1.76 ± 0.07 μm, corresponding to an equivalent radius of 0.44 μm (Table 1), was longer than that of *P. flu* CHA19-WS cells, 1.44 ± 0.03 μm, which corresponded to an equivalent radius of 0.41 μm (Table 1), a finding that was confirmed by SEM images (Figure 1). In addition, under the experimental conditions of 10 mM NaCl, pH 6.0–6.2, the two strains displayed statistically different ($p = 1.9 \times 10^{-4}$) negative

zeta potential values, -18.78 ± 1.31 mV and -16.22 ± 0.89 mV for *P. flu* CHA0 and *P. flu* CHA19-WS, respectively.

Figure 2 shows a TEM image of rod-shaped CNC particles with a length of 100–200 nm and a width (diameter) of around 10 nm; the hydrodynamic diameter (length) of the CNC particles measured using DLS was 114 ± 2.13 nm, which corresponds to an equivalent radius of 0.020 μm (Table 1). The zeta potential of the CNC particles in 10 mM NaCl, pH 6.0–6.2, was -42.3 ± 1.07 mV, indicating negatively charged surfaces that can be attributed to the sulfate ester groups introduced by the esterification reaction during hydrolysis.

Bacterial aggregation

Without CNC, the two strains were well dispersed (Figures S1 A and C), free of flocculate (average radius = 0.44 μm and 0.41 μm for *P. flu* CHA0 and *P. flu* CHA19-WS, respectively, calculated based on DLS measurements), and the culture chamber liquid was observed to be turbid. With the addition of CNC, *P. flu* CHA19-WS showed significant aggregation and formed large, dense bacterial aggregates (estimated average radius = 4.5 μm) (Figure S1 D), while *P. flu* CHA0 formed small, loose bacterial aggregates (estimated average radius = 2 μm) (Figure S1 B). The results indicate that, although bacterial cells can spontaneously form flocs, bacterial flocs were unlikely to form without CNC application under the experimental conditions tested here.

To determine the interaction between bacterial cells and CNC particles, zeta potential distributions of bacteria, of CNC, and of a mixture of bacteria and CNC were measured under the same physicochemical conditions. The measurement of zeta potential

distributions of individual components and their combination to study particle interactions follows the work of [22]. As shown in Figure S2 A, samples with only CNC particles exhibited single modal zeta potential distributions, with peaks at ~ -40 mV. Samples with only bacterial strains also exhibited single modal zeta potential distributions, with peaks at ~ -17 mV and ~ -15 mV for *P. flu* CHA0 (Figure S2 B) and *P. flu* CHA19-WS (Figure S2 C), respectively. A bimodal zeta potential distribution was observed for samples with a mixture of CNC and bacterial cells, with a peak at ~ -40 mV representing CNC particles and a peak at ~ -17 mV representing *P. flu* CHA0 (Figure S2 D), a peak at ~ -15 mV representing *P. flu* CHA19-WS (Figure S2 E). The zeta potential results suggest that bacterial cells and CNC have no direct contact with each other under the conditions tested. This observation implies that depletion interactions play a key role in the observed bacterial aggregation in the presence of CNC. However, the impact of physicochemical factors (e.g., pH, ionic strength, CNC concentration) on CNC-induced bacterial aggregation deserves further research.

Batch bacterial initial adhesion

Figure 3 illustrates the enumeration of the cell density of each strain deposited on glass cover slips, determined from microscopic observations. As can be seen in Figure 3, in the absence of CNC, *P. flu* CHA19-WS showed a slightly higher ($p = 0.049$) adhesion capability (average $1.02 \times 10^6 \pm 3.85 \times 10^5$ cells·cm^{-2}) than did *P. flu* CHA0 (average $7.40 \times 10^5 \pm 1.84 \times 10^5$ cells·cm^{-2}), which might be explained by the fact that *P. flu* CHA19-WS is less negatively charged than the wild type *P. flu* CHA0. It should also be noted that the higher EPS coverage of the *P. flu* CHA19-WS strain, in comparison to its

wide type strain, might play an important role in controlling its initial adhesion to glass surfaces. In a bacterial adhesion kinetic study using a radial stagnation point flow system, [5] indicated that a greater bacterial adhesion to a quartz surface resulted from more EPS coverage.

After the addition of CNC, deposition of *P. flu* CHA0 (average 2.07×10^5 cells·cm^{-2}) and *P. flu* CHA19-WS (average 8.69×10^4 cells·cm^{-2}) on glass cover slips was significantly ($p = 7.72 \times 10^{-8}$ and 4.49×10^{-7}, respectively) inhibited, and achieved about 0.6 (~ 72%) and 1.1 log-unit reduction (~ 91.5%) in cell density, respectively.

Bacterial initial adhesion under continuous flow conditions

Bacterial initial adhesion under continuous flow conditions (flow rate = 0.15 mL·min^{-1}) was studied using a QCM-D coupled with a fluorescence microscope. QCM-D frequency shifts (ΔF) and dissipation changes (ΔD) with time were monitored, where a large ΔF suggests a large mass load on silica surfaces and a large ΔD suggests a soft mass load on silica surfaces.

As shown in Figure 4A, adsorption began as soon as the sample solution made contact with the silica surface. In the absence of bacteria, CNC adsorption on silica reached a plateau of around 1.75 Hz about 50 min post-CNC injection. In approximately 55 minutes, *P. flu* CHA0 achieved a ΔF of around 4.5 Hz without CNC and a ΔF of 1.75 Hz with CNC, a value the same as that of CNC alone. The finding that the ΔF of *P. flu* CHA0 supplemented with CNC was lower than that of *P. flu* CHA0 alone, indicates that *P. flu* CHA0 adhesion to a silica surface was inhibited by CNC. Adsorbed CNC and *P. flu* CHA0 supplemented with CNC desorbed slightly upon rinsing with 10 mM NaCl. In

the absence of CNC, adsorbed *P. flu* CHA0 desorbed significantly and reached a final ΔF of around 4 Hz. The desorption of *P. flu* CHA0 suggests that these bacteria had been reversibly deposited on the silica surface.

Similarly, the ΔD began to change as soon as the sample made contact with the silica surface (Figure 4A). It should be noted that dissipation occurs when the driving voltage to the crystal is shut off and the energy from the oscillating crystal dissipates from the system. ΔD indicates the energy dissipation (loss of energy/damping) response of the freely oscillating sensor, which corresponds to the viscoelastic properties of the adsorbed molecular layers on the quartz surface (Equation 4 in the Supporting Information). A final ΔD of around 0.15×10^{-6} for both CNC and *P. flu* CHA0 supplemented with CNC was achieved. The final ΔD of *P. flu* CHA0 was around 0.5×10^{-6}. This suggests that the binding of attached *P. flu* CHA0 cells to the silica surface was relatively more flexible than the binding of *P. flu* CHA0 supplemented with CNC, where the cell is not coupled so closely to the surface, highlighting the viscoelastic nature of the attached bacterial cells [23].

The adsorption of *P. flu* CHA19-WS achieved a final ΔF around 5 Hz (Figure 4B), and desorbed only slightly upon rinsing with 10 mM NaCl. Consistent with the batch adhesion results (Figure 3), *P. flu* CHA19-WS (Figure 4B) showed a slightly higher adhesion capability than that of *P. flu* CHA0 (Figure 4A) under the same hydrodynamic flow condition. ΔF of the *P. flu* CHA19-WS supplemented with CNC was around 0.2 Hz and decreased to around 0 Hz when rinsed with 10 mM NaCl, indicating that few *P. flu* CHA19-WS cells were adsorbed on the silica surface and that the adsorption was loose.

A final ΔD of about 0.35×10^{-6} was achieved with *P. flu* CHA19-WS and a final ΔD of about 0 was observed for *P. flu* CHA19-WS supplemented with CNC. This suggests a relatively more rigid binding of attached *P. flu* CHA19-WS cells supplemented with CNC to the silica surface, compared with *P. flu* CHA19-WS cells only.

Because it is difficult to directly link ΔF in QCM-D to the numbers of the attached bacterial cells [9, 12, 14], microscopy was employed to quantify cell numbers of bacteria adhered to the silica surfaces to support ΔF results in QCM-D bacterial adhesion studies. Microscopy images of the silica surfaces were captured after each QCM-D adhesion experiment, and the cell density on silica surfaces was calculated (Figure 4C) based on the microscopy images. As shown in Figure 4C, adhesion of *P. flu* CHA0 (~ 5.96×10^5 cells·cm^{-2}) on silica surfaces was significantly ($p < 0.05$) inhibited by CNC (to ~ 6.87×10^4 cells·cm^{-2}, or ~ 88.5% inhibition), which was consistent with the *P. flu* CHA0 QCM-D adhesion results. The cell density of *P. flu* CHA19-WS on the silica surface (~ 1.36×10^6 cells·cm^{-2}) was higher than that of *P. flu* CHA0 (~ 5.96×10^5 cells·cm^{-2}), which is consistent with the batch (Figure 3) and QCM-D adhesion results (Figures 4A and 4B). In the presence of CNC, adsorption of *P. flu* CHA19-WS was also significantly ($p < 0.05$) hindered (to ~ 9.25×10^4 cells·cm^{-2}, or ~ 93.2% inhibition), as determined from microscopic observations (Figure 4C), although the final ΔF of the *P. flu* CHA19-WS supplemented with CNC was about 0 in QCM-D experiments (Figure 4B), which might be associated with the presence of EPS and surface hydrophobicity, as these factors have been reported to lead to a reduced ΔF in QCM-D results [12, 14]. Therefore, it is necessary to use direct microscopy to support ΔF results in QCM-D bacterial adhesion studies [9, 12, 14].

Classic DLVO interactions

Experimentally measured equivalent radii and zeta potential values were used in the DLVO interaction energy calculations (Table 1). The primary energy minimum (Φ_{1min}), the primary energy barrier (Φ_{max}), and the secondary energy minimum (Φ_{2min}) are presented in Table 1. The DLVO energy profile is depicted in Figure S3 in the Supporting Information. A negative Φ at the primary energy minimum or secondary energy minimum indicates attractive forces that contribute to colloidal attachment whereas a positive Φ suggests a repulsive force that promotes colloidal stability or mobility. Although an idealized DLVO approach was applied by assuming bacterial cells and CNC particles were smooth spheres, the energy calculations can be considered to capture the qualitative trends of the samples.

Figure S3 shows the energy sum of the electrostatic and van der Waals interactions, both of which decay with separation distance. Without CNC, the strong positive repulsive energy barriers of *P. flu* CHA0 (202 kT) and *P. flu* CHA19-WS (118 kT) to the silica surface interactions indicate that the adhesion of both cell types to the silica surface was unfavorable. This was expected because the surface of both bacterial cells and silica surface were negatively charged under most physiological conditions, giving rise to repulsive electrostatic interactions on close approach. Previous studies reported that bacterial adhesion to solid surfaces (for instance, sand grains) occurred in the presence of sizable calculated primary energy barriers up to 1000 kT, likely due to the local surface charge heterogeneities on collector surfaces, which are not accounted for by classical DLVO theory [24, 25]. Additionally, the presence of shear force in both batch and QCM-D systems in the current study might also contribute to an unfavorable condition for

bacterial deposition. In the present study, bacterial adhesion occurred under both batch (Figure 3) and hydrodynamic flow (Figure 4) conditions, suggesting bacterial adhesion studied here might be attributed to the primary minima. Of note, the secondary minima of both bacterial strains were around -4.6 kT, which are higher than the average thermal energy of the Brownian particles themselves (~ 1.5 kT) [26]. Thus, deposition in secondary minima for both strains was not negligible. The depths of primary minima and secondary minima of both bacteria were close to each other, suggesting that the theoretical DLVO energy profile (Figure S3) could not explain the observed difference in adhesion abilities of the two bacterial strains (Figures 3 and 4). The presence of shear force and different EPS coverage (*P. flu* CHA19-WS has increased EPS production than *P. flu* CHA0, Figure 1) might explain the different adhesion abilities. *P. flu* CHA0 cells with a hydrodynamic diameter of 1.76 ± 0.07 μm, corresponding to an equivalent radius of 0.44 μm (Table 1), were bigger than *P. flu* CHA19-WS cells with a hydrodynamic diameter of 1.44 ± 0.03 μm, corresponding to an equivalent radius of 0.41 μm (Table 1); thus, *P. flu* CHA0 cells may experience a larger shear force and thus be less easily deposited than *P. flu* CHA19-WS cells.

With the addition of CNC, DLVO predicted deep primary minima (-9293 kT for *P. flu* CHA19-WS and -3907 kT for *P. flu* CHA0) and secondary minima (-50 kT for *P. flu* CHA19-WS and -20.9 kT for *P. flu* CHA0) for both bacterial cells to the silica surface, indicating that more cell deposition was expected than was observed in our adhesion results. This deviation might be explained by the fact that the larger-sized bacterial aggregates formed in the presence of CNC could experience reduced convective-diffusive transport to the solid surface, resulting in their reduced deposition on the surface.

In the case of CNC particles only, a positive energy barrier about 10 kT was predicted. Although CNC particles and the silica surface were both negatively charged, it is possible for some CNC particles to deposit on the silica surface irreversibly in the primary minimum due to the small primary energy barrier. The QCM-D study showed an obvious deposition of CNC on the silica surface, and those previously deposited CNC was only partially removed after Milli-Q water injection (Figure S4), indicating that CNC adhesion was mainly attributed to the primary minimum, and CNC might also interact with the silica surface at a small separation distance (around 15 nm), due to the presence of the reversible secondary minimum (-1.9 kT).

Bacterial cells may also experience steric, hydration, and hydrodynamic forces when approaching a silica surface. Surface roughness or surface charge heterogeneity [13, 16, 27, 28] of both bacterial and silica surfaces may represent other explanations for deviation of the observed bacterial adhesion behaviors from predicted DLVO curves. Furthermore, the zeta potential of the silica surface might have changed due to the deposition of CNC. However, it is challenging to evaluate the distribution of CNC on the silica surface, and the reference zeta potential values used in the classic DLVO interaction calculations are likely to be inaccurate.

Discussion

Impact of CNC on bacterial aggregation

Our studies showed that CNC particles induce bacterial aggregation mainly through depletion interactions. Based on the depletion mechanism, the addition of repulsive CNC particles into a dispersion of bigger colloidal bacterial cells might destabilize the system

[29]. Theoretical calculations of the depletion potential W for bacterial cells in the presence of rod-shaped CNC particles are given as (detailed calculations are provided in the Supporting Information):

$$W(h) = -\frac{2}{3} k_B \mathrm{T} \varphi_r \frac{L}{D} \frac{R}{D} (1 - \frac{h}{L})^3 \quad (3)$$

where k_B is the Boltzmann constant, T is the absolute temperature, L is the length, D is the diameter, φ_r is the volume fraction of rod-shaped particles (CNC particles), R is the diameter, and h is the surface-to-surface distance of bigger spherical colloidal particles (bacterial cells). The result indicates that under the test conditions in this study, depletion aggregation was unlikely to occur due to the low CNC concentration in the system (3.3×10^{-3} mL·mL^{-1}); based on the model prediction, a volume fraction φ_r of 1×10^{-2} mL·mL^{-1} is needed for aggregation. There are three possible explanations for the observed deviation of the aggregation from predicted depletion potentials.

First, the formula (Equation 3) used in the depletion potential calculations is ideal for large spherical particles in the presence of small, rod-shaped particles, whereas the bacterial cells in the current study were cylindrically shaped. Second, the deviation might be explained by the presence of bacterial EPS which could impose polymer-mediated steric interactions such as polymer bridging that were not considered in the predicted depletion potentials. Eboigbodin et al. (2005) showed that EPS were involved in a depletion attractive mechanism, which induced bacterial aggregation and phase separation of *Escherichia coli* cells. Previous studies [30, 31] have shown that EPS surrounding the bacterial cells can trigger a depletion interaction among the bacterial cells. Repulsive interactions between like-charged bacterial cells can lead to depletion,

whereas the presence of EPS can impose polymer bridging [32], resulting in more significant aggregation of the more EPS-covered strain (*P. flu* CHA19-WS in our study). As polymer induced forces are sensitive to the ionic strength of the solution [33, 34], the impact of polymer bridging on bacterial adhesion in the presence of CNC under different ionic strength conditions should be investigated. Third, the surface charge of bacterial cells might play an important role in bacterial aggregation [35]. In a previous study [6], CNC induced much more significant aggregation of *P. aeruginosa* PAO1 than was observed in the two *P. fluorescens* strains in the current study. The *P. aeruginosa* PAO1 used in the previous study was more negatively charged (-29.84 mV in 10 mM NaCl, pH 6.0–6.2) than the *P. fluorescens* strains (-18.78 and -16.22 mV for *P. flu* CHA0 and *P. flu* CHA19-WS, respectively in 10 mM NaCl, pH 6.0–6.2) used in this study.

Impact of CNC on bacterial initial adhesion

In the presence of CNC, a significant reduction in bacterial initial adhesion on glass surfaces was observed using both batch and continuous flow methods, suggesting that CNC is capable of reducing bacterial initial adhesion to a solid surface. It was also observed that the extent of CNC-induced reduction in bacterial initial adhesion varied depending on the bacterial surface EPS coverage. There are several potential explanations for the above observations.

First, compared to single bacterial cells, the larger-sized bacterial aggregates formed in the presence of CNC could experience reduced convective-diffusive transport to the solid surface, resulting in their reduced deposition on the surface. Based on the dimensions and flow rates employed in the QCM-D flow cell, the *Pe* number was estimated to be 0.001

[13], indicating that the bacteria in the QCM-D flow cell effectively experienced a diffusion-dominated flow regime [36, 37]. Therefore, the decrease in diffusion coefficient with increasing colloid size that led to reduced bacterial deposition in the presence of CNC, could also hold true for the QCM-D flow cell.

The extent of bacterial deposition reduction varied depending on the bacterial surface EPS coverage. In the presence of CNC, bacteria with more EPS formed relatively larger flocs compared to bacteria with less EPS (Figures S1 D and B), resulting less bacterial initial adhesion under both batch (Figure 3) and continuous flow conditions (Figure 4C).

Second, in the presence of CNC, larger bacterial aggregates experience greater shear force along the solid surface than do nonaggregated cells; an increased shear force might lead to a greater detachment rate. The shear force under hydrodynamic flow conditions likely sweeps attached secondary minimum associated bacteria from the system [28].

Third, adsorption of negatively charged CNC particles on silica surfaces contributes repulsive electrostatic and steric forces that can reduce the deposition of bacterial cells and enhance the reentrainment of deposited bacterial cells to the bulk liquid. CNC adsorption on silica surfaces increased the surface negativity (-42.3 ± 1.07 mV and -36.3 ± 0.15 mV in 10 mM NaCl, pH 6.0–6.2, for CNC and the silica surface, respectively). Deposition of bacterial cells might be hindered due to the enhanced repulsive forces between the bacterial cells and the CNC coated silica surfaces. This hypothesis was supported by our QCM-D study that showed no more bacterial adhesion on CNC coated silica surface (Figure S4).

Fourth, the presence of CNC may lead to a bacterial EPS conformational change that inhibits EPS interaction with solid surfaces. Chen and colleagues [5] reported that due to

the presence of certain ions, bacterial surface polymers may become more rigid and thus be inhibited from interacting with a quartz surface. This rigidity minimized the ability of the polymers to reconform to and interact directly with a solid surface. In our study, the antibacterial adhesion effects of CNC were more pronounced for bacterial cells with greater EPS coverage, indicating that EPS play a significant role in controlling bacterial interactions with CNC and other bacteria. However, further experiments that test the impact of CNC on bacterial surface polymers are needed to evaluate this hypothesis.

Other potential mechanisms should also be considered. For instance, with an increase of bacterial size, gravitational settling probably increases resulting in more bacterial deposition on silica surfaces. A previous study showed that gravitational dominance can be expected for particles greater than 1 μm in diameter [38]. In the present study, the equivalent spherical diameter of bacterial cells increased from ~ 0.8 μm in the absence of CNC to 4 μm and 9 μm in the presence of CNC for *P. flu* CHA0 and *P. flu* CHA19-WS, respectively. Our results indicate that gravitational sedimentation did not play a significant role in controlling bacterial initial adhesion under the conditions in this study. Other interaction forces, such as the shear force may play a more important role and lead to reduced bacterial adhesion in the presence of CNC. Further research on the impact of flow conditions (such as flow rate) and physicochemical factors (such as pH and ionic strength) on bacterial adhesion in the presence of CNC will provide better understanding of the mechanisms in CNC-reduced bacterial initial adhesion.

Conclusion

This study indicates that CNC can induce bacterial aggregation, and thus inhibit subsequent bacterial initial adhesion on solid surfaces. Under the batch and hydrodynamic flow conditions applied, the effect of CNC on bacterial aggregation caused a significant reduction in bacterial initial adhesion to silica surfaces. Thus, CNC might be an excellent candidate for creation and manipulation of bacterial flocs and for preventing bacterial initial adhesion and subsequent biofilm development. Artificial formation of bioflocs and control of the development of biofilms are of interest in many applications involving biodegradation or bioremediation [39].

Acknowledgements

Authors X. Sun and Y. Liu thank the Natural Sciences and Engineering Research Council of Canada (NSERC) for support of this project. We thank Professor Howard Ceri in the Biological Sciences Department, University of Calgary, for providing bacterial strains. We thank Dr. Hongbo Zeng, University of Alberta, for help with the zeta potential analysis, and Ms. Arlene Oatway in the Microscopy Unit, University of Alberta, for taking SEM and TEM images.

References

[1] T. Mattilasandholm, G. Wirtanen *Food Reviews International*. **1992**, 8, 573-603.

[2] Y. Liang, N. Hilal, P. Langston, V. Starov *Advances in Colloid and Interface Science*. **2007**, 134-35, 151-166.

[3] Q. Y. Lu, J. Wang, A. Faghihnejad, H. B. Zeng, Y. Liu *Soft Matter*. **2011**, 7, 9366-9379.

[4] R. Bos, H. C. van der Mei, H. J. Busscher *Fems Microbiology Reviews*. **1999**, 23, 179-230.

[5] G. X. Chen, S. L. Walker *Langmuir*. **2007**, 23, 7162-7169.

[6] X. H. Sun, C. Danumah, Y. Liu, Y. Boluk *Chemical Engineering Journal*. **2012**, 198, 476-481.

[7] S. Asakura, F. Oosawa *Journal of Polymer Science*. **1958**, 33, 183-192.

[8] K. Otto, H. Elwing, M. Hermansson *Journal of Bacteriology*. **1999**, 181, 5210-5218.

[9] A. L. J. Olsson, H. C. van der Mei, H. J. Busscher, P. K. Sharma *Journal of Colloid and Interface Science*. **2011**, 357, 135-138.

[10] J. Strauss, Y. T. Liu, T. A. Camesano *Jom*. **2009**, 61, 71-74.

[11] A. L. J. Olsson, H. C. van der Mei, H. J. Busscher, P. K. Sharma *Langmuir*. **2010**, 26, 11113-11117.

[12] I. M. Marcus, M. Herzberg, S. L. Walker, V. Freger *Langmuir*. **2012**, 28, 6396-6402.

[13] N. Vanoyan, S. L. Walker, O. Gillor, M. Herzberg *Langmuir*. **2010**, 26, 12089-12094.

[14] J. Gutman, S. L. Walker, V. Freger, M. Herzberg *Environmental Science & Technology*. **2013**, 47, 398-404.

[15] N. I. Abu-Lail, T. A. Camesano *Environmental Science & Technology*. **2003**, 37, 2173-2183.

[16] S. L. Walker, J. A. Redman, M. Elimelech *Langmuir*. **2004**, 20, 7736-7746.

[17] S. Bayoudh, A. Othmane, L. Mora, H. Ben Ouada *Colloids and Surfaces B-Biointerfaces*. **2009**, 73, 1-9.

[18] E. J. W. Verwey *Journal of Physical and Colloid Chemistry*. **1947**, 51, 631-636.

[19] M. C. W. Smith *Journal of the American Chemical Society*. **1983**, 105, 2510-2510.

[20] B. Derjaguin, L. Landau *Progress in Surface Science*. **1993**, 43, 30-59.

[21] M. L. Workentine, J. J. Harrison, V. Tran, P. U. Stenroos, A. M. Weljie, P. Zhang, H. J. Vogel, H. Ceri, R. J. Turner. **2008**. http://stahl.ce.washington.edu/internal/downloadable/meetings/asm2008/data/papers/K-160.htm

[22] Z. H. Xu, J. J. Liu, J. W. Choung, Z. A. Zhou *International Journal of Mineral Processing*. **2003**, 68, 183-196.

[23] C. Poitras, N. Tufenkji *Biosensors & Bioelectronics*. **2009**, 24, 2137-2142.

[24] S. E. Truesdail, J. Lukasik, S. R. Farrah, D. O. Shah, R. B. Dickinson *Journal of Colloid and Interface Science*. **1998**, 203, 369-378.

[25] J. A. Redman, S. L. Walker, M. Elimelech *Environmental Science & Technology*. **2004**, 38, 1777-1785.

[26] M. W. Hahn, C. R. O'Melia *Environmental Science & Technology*. **2004**, 38, 210-220.

[27] Y. S. Li, Y. G. Wang, K. D. Pennell, L. M. Abriola *Environmental Science & Technology*. **2008**, 42, 7174-7180.

[28] W. P. Johnson, M. P. Tong *Environmental Science & Technology*. **2006**, 40, 5015-5021.

[29] A. Vrij *Pure and Applied Chemistry*. **1976**, 48, 471-483.

[30] S. Tsuneda, H. Aikawa, H. Hayashi, A. Hirata *Journal of Colloid and Interface Science*. **2004**, 279, 410-417.

[31] K. E. Eboigbodin, J. R. A. Newton, A. F. Routh, C. A. Biggs *Langmuir*. **2005**, 21, 12315-12319.

[32] S. P. Strand, M. S. Vandvik, K. M. Varum, K. Ostgaard *Biomacromolecules*. **2001**, 2, 126-133.

[33] H. N. Kim, Y. Hong, I. Lee, S. A. Bradford, S. L. Walker *Biomacromolecules*. **2009**, 10, 2556-2564.

[34] H. N. Kim, S. L. Walker, S. A. Bradford *Water Research*. **2010**, 44, 1082-1093.

[35] H. Wang, M. Sodagari, Y. J. Chen, X. He, B. M. Z. Newby, L. K. Ju *Colloids and Surfaces B-Biointerfaces*. **2011**, 87, 415-422.

[36] I. R. Quevedo, N. Tufenkji *Environmental Science & Technology*. **2009**, 43, 3176-3182.

[37] M. Elimelech, X. Jia, J. Gregory, R. Williams, Particle deposition and aggregation: measurement, modelling and simulation, Butterworth-Heinemann, Oxford, UK., **1995**.

[38] G. X. Chen, Y. S. Hong, S. L. Walker *Langmuir*. **2010**, 26, 314-319.

[39] A. Kumar, N. P. Mortensen, P. P. Mukherjee, S. T. Retterer, M. J. Doktycz *Applied Physics Letters*. **2011**, 98.

Figure 1 Representative SEM micrographs of (A) *P. flu* CHA0 and (B) *P. flu* CHA19-WS

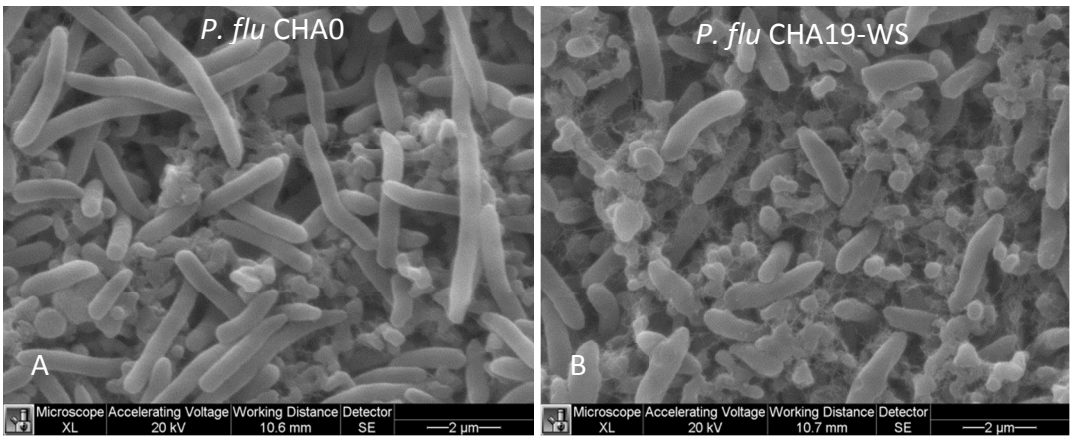

Figure 2 TEM image of CNC particles (Bar size = 200 nm)

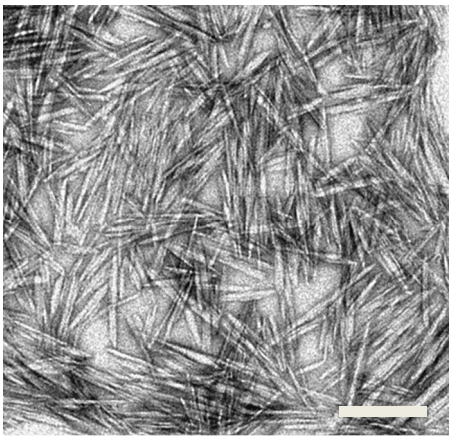

Figure 3 Enumeration of batch bacterial adhesion studies. Each data point represents the average of three measurements for one sample. Error bars represent the standard deviation.

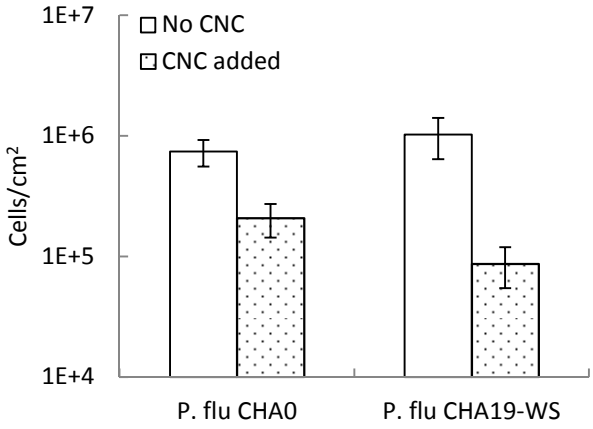

Figure 4 Representative QCM-D adhesion results (The frequency change ΔF and dissipation change ΔD responses for the adsorption of CNC, bacteria with CNC and bacteria respectively obtained from QCM-D measurements. Solutions were sequentially pumped through the SiO_2 sensor surface in the following order: 10 mM NaCl (0-10 min, flat line in the figure), samples (CNC, mixture of bacteria and CNC, bacteria) in 10 mM NaCl (starting from the arrowed position), and 10 mM NaCl (starting from the arrowed position) at 0.15 mL/min.) (A) Adsorption profile of *P. flu* CHA0 with and without CNC; (B) Adsorption profile of *P. flu* CHA19-WS with and without CNC; (C) Cell density (cells/cm^2) on silica surface after QCM-D adhesion experiments. Each data point represents the average of three measurements for one sample. Error bars represent the standard deviation.

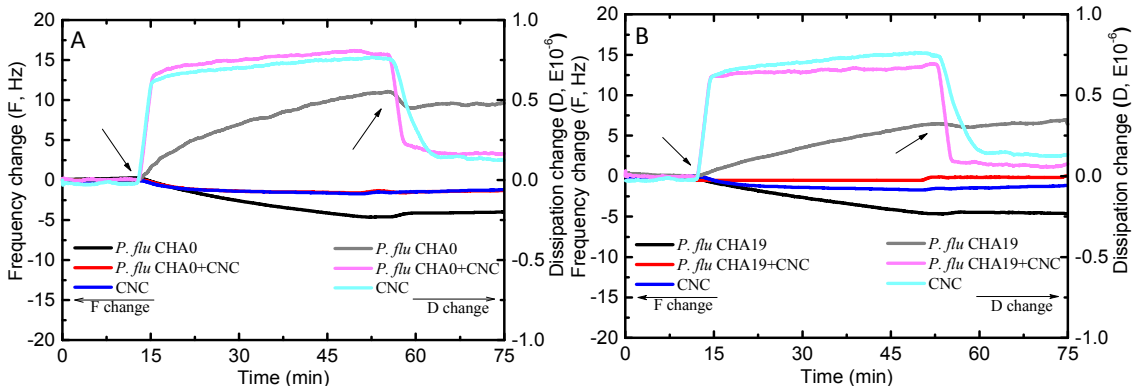

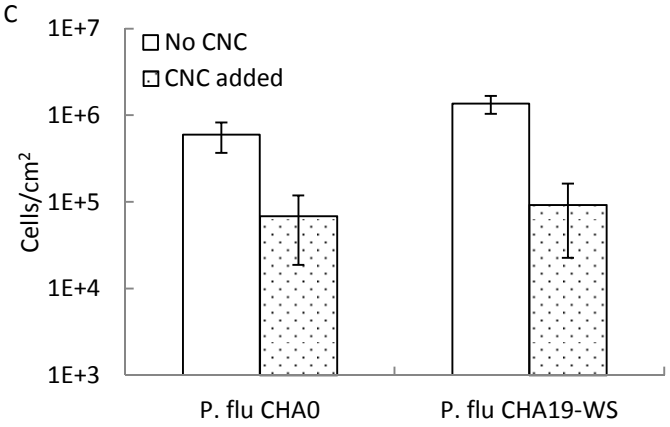

Table 1 Key parameters used in DLVO calculations and interaction energies as calculated by DLVO theory

Sample	Size[a](μm) DLS	Size[a](μm) Equivalent Radii	Zeta potential[b] (mV)	Φ_{1min}[c] (kT)	Φ_{max}[d] (kT)	Φ_{2min}[e] (kT)
P. flu CHA0	1.76±0.07	0.44	-18.78±1.31	-860	202	-4.6
P. flu CHA0+CNC	N/A	2.0	-18.78±1.31	-3907	920	-20.9
P. flu CHA19-WS	1.44±0.03	0.41	-16.22±0.89	-847	118	-4.6
P. flu CHA19-WS+CNC	N/A	4.5	-16.22±0.89	-9293	1299	-50
CNC	0.114±0.002	0.020	-42.30±1.07	-319.0	10.0	-1.9

a. The average particle hydrodynamic size, determined by DLS.
   Note: aggregates size of *P. flu* CHA0, and *P. flu* CHA19-WS after addition of CNC was determined by microscopy.
b. Zeta potential was tested in 10 mM NaCl solution (pH 6.0-6.2).
c. The depth of the primary energy minimum, calculated by DLVO theory.
d. The height of the primary energy barrier, calculated by DLVO theory.
e. The depth of the secondary energy minimum, calculated by DLVO theory.